# Retinotopic Organization of Primary Visual Cortex in Glaucoma: A Method for Comparing Cortical Function with Damage to the Optic Disk

*Robert O. Duncan, Pamela A. Sample, Robert N. Weinreb, Christopher Bowd, and Linda M. Zangwill*

**Purpose.** To demonstrate that the relationship between the functional organization of primary visual cortex (V1) and damage to the optic disc in humans with primary open-angle glaucoma (POAG) can be measured using a novel method for projecting scotomas onto the flattened cortical representation.

**Methods.** Six subjects participated in this functional magnetic resonance imaging (fMRI) experiment. Structural damage to the optic disc and the retinal nerve fiber layer (RNFL) was measured by three techniques: scanning laser polarimetry (GDx ECC; Carl Zeiss Meditec, Dublin, CA), confocal scanning laser ophthalmoscopy (HRT II; Heidelberg Engineering, Heidelberg, Germany), and optical coherence tomography (StratusOCT; Carl Zeiss Meditec, Inc.). Cortical activity for viewing through the glaucomatous versus fellow eye was compared by alternately presenting each eye with a contrast-reversing checkerboard pattern. The resultant fMRI response was compared to interocular differences in RNFL or mean height contour for analogous regions of the visual field.

**Results.** fMRI responses to visual stimulation were related to differences in RNFL thickness or mean height contour between eyes. The correlation between fMRI responses and measurements of optic disc damage for OCT (RNFL), HRT (mean height contour), and GDx (RNFL) were $r = 0.90$ ($P = 0.02$), $r = 0.84$ ($P = 0.04$), and $r = 0.79$ ($P = 0.063$), respectively. The probability of observing all three correlations by chance was low ($P = 0.0003$).

**Conclusions.** Cortical activity in human V1 was altered in these six POAG subjects in a manner consistent with damage to the optic disc. fMRI is a possible means for quantifying cortical neurodegeneration in POAG. (*Invest Ophthalmol Vis Sci.* 2007;48:733–744) DOI:10.1167/iovs.06-0773

Glaucoma is the second leading cause of blindness worldwide, and will affect more than 3 million Americans by 2020.[1] Although intraocular pressure (IOP) is a known leading risk factor for glaucoma, the pathophysiology of neurodegeneration in the disease is unknown. Glaucoma often causes vision loss in subjects with normal IOP, demonstrating that there are additional factors that contribute to the disease.[2]

Understanding brain changes in human glaucoma may provide insights into the pathobiology of the disease. Recently, it has been determined that the death of retinal ganglion cells adversely affects the optic nerve,[3,4] the lateral geniculate nucleus (LGN) of the thalamus,[4–6] and primary visual cortex (V1).[7,8] Although multifocal visually evoked potentials (mfVEPs) have been used successfully to measure glaucomatous neural activity objectively in vivo,[9–17] the technique is restricted by the fact that signals cannot be accurately localized to specific brain regions.[18] Evidence of glaucomatous damage in the brain has also been demonstrated in vivo using positron emission tomography (PET),[19] and single photon emission computed tomography (SPECT).[20,21] However, PET and SPECT have poor spatial resolution and are not practical for repeatedly monitoring glaucomatous progression, because they require radioisotopes.

Functional magnetic resonance imaging (fMRI) has rapidly become the standard for inferring neuronal activity in human subjects. Increases in neuronal activity are accompanied by changes in blood oxygenation that give rise to changes in the MR signal. This blood oxygenation level–dependent (BOLD) signal serves as the basis for a majority of studies that measure brain function in vivo. To date, the effects of optic neuropathy on the occipital cortex of humans have been investigated in only one fMRI study, and the techniques used were not optimal.[22] Unfortunately, the methodology used in that study resulted in poor response localization, and neuronal and behavioral responses were not compared. Despite these shortcomings, fMRI is better suited to measuring glaucomatous neuronal activity than are other brain imaging methods, because (1) it is relatively noninvasive compared with methods that require isotope (PET and SPECT); (2) fMRI affords better spatial resolution and localization than mfVEP, PET, or SPECT; and (3) fMRI, unlike traditional $T_1$-weighted MRI, has the ability to look at function-specific neuronal activity associated with the loss of retinal ganglion cell subtypes in glaucoma. For these reasons, fMRI is a potentially useful means of measuring postretinal neurodegeneration in human glaucoma. However, it must first be determined whether fMRI measurements of glaucomatous neurodegeneration correlate with accepted measures of damage to the optic nerve.

Preliminary studies by our group suggest that the pattern of cortical activity in V1 may be correlated with the pattern of visual field loss measured with automated perimetry.[23] Still, behavioral reports of visual function may not be as sensitive in some patients as structural measurements of the optic disc or assessment of the retinal nerve fiber layer (RNFL). Indeed, a majority of the retinal ganglion cells may already be dead by the time visual field defects are detected in some individuals by standard perimetric techniques.[24,25] Consequently, this study was designed to quantify the relationship between damage to the optic disc, the thickness of the RNFL, and neuronal activity

From the Hamilton Glaucoma Center, Department of Ophthalmology, University of California, San Diego, California.

Supported by National Eye Institute Grants EY08208 (PAS) and EY11008 (LMZ). Participant retention incentive grants in the form of glaucoma medication at no cost: Alcon Laboratories Inc., Allergan, Pfizer Inc., and Santen, Inc.

Submitted for publication July 7, 2006; revised September 13, 2006; accepted December 18, 2006.

Disclosure: **R.O. Duncan**, None; **P.A. Sample**, Carl Zeiss Meditec, Welch-Allyn, Haag Streit (F); **R.N. Weinreb**, Carl Zeiss Meditec (F, R); **L.M. Zangwill**, Carl Zeiss Meditec, Heidelberg Engineering (F, R)

The publication costs of this article were defrayed in part by page charge payment. This article must therefore be marked "*advertisement*" in accordance with 18 U.S.C. §1734 solely to indicate this fact.

Corresponding author: Robert O. Duncan, Hamilton Glaucoma Center, Department of Ophthalmology, University of California, San Diego, 9500 Gilman Dr., Dept. 0946, La Jolla, CA 92093-0946; rduncan@eyecenter.ucsd.edu.

in V1 in patients with asymmetric glaucomatous visual field damage.

## METHODS

### Subjects

Six subjects with asymmetric primary open-angle glaucoma (POAG) with one glaucomatous eye and a less affected contralateral eye were included. Subjects were evaluated at the Hamilton Glaucoma Center, Department of Ophthalmology, University of California San Diego (UCSD) between July 2004 and August 2005. The subjects in this cross-sectional study were recruited from a longitudinal study designed to evaluate the optic nerve structure and visual function in glaucoma (Diagnostic Innovations in Glaucoma Study; DIGS). An experienced neuroradiologist reviewed the anatomic reference volumes for evidence of untoward disease along the retinocortical pathway, and found no evidence of tumors, compression of the optic nerve, or other diseases that could present as glaucoma. A summary of relevant subject data appears in Table 1.

### Inclusion–Exclusion Criteria

All subjects underwent complete ophthalmic examination including slit lamp biomicroscopy, intraocular pressure measurement, dilated stereoscopic fundus examination, and stereophotographs of the optic nerve heads. Good-quality simultaneous stereoscopic photographs were obtained for all subjects. All subjects had open angles, a best corrected acuity of 20/40 or better, a spherical refraction within +5.0 D, and cylinder correction within +3.0 D. A family history of glaucoma was allowed. Informed consent was obtained from all subjects, and the UCSD Internal Review Board approved all methods pertaining to human subjects. The study adhered to the Declaration of Helsinki for research involving human subjects.

Subjects did not have a history of intraocular surgery (except for uncomplicated glaucoma or cataract surgery), secondary causes of elevated IOP (e.g., iridocyclitis, trauma), other intraocular eye disease, other diseases affecting the visual field (e.g., pituitary lesions, demyelinating diseases, $HIV^+$ or AIDS, or diabetic retinopathy), medications known to affect visual field sensitivity, or problems other than glaucoma affecting color vision.

Evaluation of structural damage to the optic disc was based on assessment of simultaneous stereoscopic optic disc photographs (Stereo Camera Model 3-DX; Nidek Inc., Palo Alto, CA). Two experienced graders evaluated the photographs, and each grader was masked to the subject's identity, the other test results, and the other grade. All included photographs were judged to be of good quality. Discrepancies between the two graders were resolved either by consensus or by adjudication by a third experienced grader.

All subjects presented with abnormal visual field results and abnormal appearance of the optic disc based on stereophotograph review in at least one eye. Abnormal visual fields were defined as a repeatable defect in at least two consecutive visits. Abnormal optic disks were defined as having an asymmetric vertical cup-to-disc ratio more than 0.2, rim thinning, notching, excavation, or nerve fiber layer defects. Visual fields were assessed using standard automated perimetry (SAP), with the 24-2 program and the Swedish Interactive Thresholds Algorithm (SITA) on the Humphrey Visual Field Analyzer (Carl Zeiss Meditec, Inc., Dublin, CA). Assessment of visual fields was based on the number of pattern deviation (PD) points that were significantly different from the normative database at $P < 0.05$ or worse. Subject fellow eyes had markedly fewer ($\chi^2$, $P < 0.0001$) visual field locations outside normal limits relative to the glaucomatous eye.

Subjects were also screened for standard MRI exclusion criteria: no conditions pr medications known to affect cerebral metabolism, no metal in the body that could not be removed, and no history of claustrophobia.

### Optic Nerve Head and RNFL Assessment

Three instruments were used to measure optic disc topography, the neuroretinal rim, and the thickness of the RNFL[26,27]: GDx with enhanced corneal compensation (ECC)[28] (software version 5.5; Carl Zeiss Meditec Inc.), the Heidelberg Retina Tomograph (HRT) II (Software version 1.5.4; Heidelberg Engineering, Heidelberg, Germany), and StratusOCT (software version 4.0.4; Carl Zeiss Meditec, Inc.).

**Scanning Laser Polarimetry: GDx ECC.** The sensitivity of scanning laser polarimetry ultimately depends on the strength of the retinal birefringence measurement relative to optical and digital noise. Sensitivity can be enhanced using a software algorithm (ECC) that measures the birefringence of the cornea and retina concurrently,[28] as opposed to canceling out the corneal measurement with variable corneal compensation (VCC). This alternate method resulted in high-quality scans of all subjects. A baseline image, consisting of the mean of three scans, was used in the analysis.

The computerized export of the temporal-superior-nasal-inferior-temporal (TSNIT) plots on the GDx ECC printout includes the mean RNFL thickness from 64 polar sectors (5.625 deg/arc). The mean for each sector was computed along the ~3.2 mm diameter measurement circle surrounding the optic nerve head. The mean RNFL thickness for the superior (0–180°) and inferior (181–360°) retinal region was computed separately by averaging the corresponding mean sectors ($n = 32$).

**TABLE 1.** RNFL and Visual Field Data by Participant

| Subject | Age (y) | Eye | GDx ECC RNFL (μm) | HRT RNFL (μm) | HRT MHC (μm) | OCT RNFL (μm) | SAP MD | SAP PSD | BOLD *P** |
|---|---|---|---|---|---|---|---|---|---|
| 1 | 58 | $OD_F$ | 59 | 21 | 5 | 112 | −0.3 | 1.38 | 0.0002 |
| | | $OS_G$ | 53 | 14 | 11 | 82 | −6.23 | 8.57 | |
| 2 | 76 | $OD_G$ | 25 | 11 | 21 | 39 | −17.0 | 12.89 | 0.001 |
| | | $OS_F$ | 42 | 23 | 15 | 74 | −4.78 | 6.10 | |
| 3 | 68 | $OD_F$ | 45 | 20 | 27 | 73 | −4.91 | 1.97 | 0.12 |
| | | $OS_G$ | 46 | 24 | 10 | 72 | −8.69 | 6.24 | |
| 4 | 77 | $OD_G$ | 56 | 20 | 5 | 102 | −6.43 | 3.83 | 0.41 |
| | | $OS_F$ | 45 | 18 | 8 | 101 | −2.77 | 1.30 | |
| 5 | 74 | $OD_G$ | 36 | 22 | 3 | 67 | −2.41 | 1.94 | <0.0001 |
| | | $OS_F$ | 45 | 33 | 2 | 94 | −0.66 | 1.55 | |
| 6 | 63 | $OD_G$ | 33 | 12 | 28 | 44 | −14.5 | 10.83 | <0.0001 |
| | | $OS_F$ | 47 | 25 | 5 | 98 | 0.80 | 1.36 | |

G, glaucomatous eye; F, fellow eye.

* Significance of the BOLD signal for voxels within the cortical representation of the scotoma.

**Confocal Scanning Laser Ophthalmoscopy: HRT II.** RNFL thickness is automatically computed by measuring the height of the retinal rim along a contour line relative to the reference plane, which is located roughly 50 $\mu$m below the retinal surface. The HRT exports the mean RNFL thickness along the contour line in 64 polar sectors (5.625 deg/arc). Mean RNFL thickness was automatically exported and used to compute the superior (0–180°) and inferior (181–360°) retinal regions by averaging across the superior and inferior sectors, respectively. Mean height contour along the disc margin was also included in the analysis. For the HRT, mean height contour was also used because it was the best predictor of POAG in a recent multivariate analysis incorporating HRT parameters obtained at baseline.[29]

**Optical Coherence Tomography: StratusOCT.** RNFL measurements were obtained using the OCT RNFL Fast Scan Pattern. The StratusOCT's RNFL Thickness Average protocol provides RNFL thickness estimates for 12 equally spaced 30° polar sectors. The mean RNFL thickness for the superior (15–165°) and inferior (195–345°) retinal regions were computed by averaging the five sectors that resided completely above or below the horizontal midline. Two sectors corresponding to the extreme nasal and temporal retinal region were excluded from the analysis because they straddled the midline.

**Quality Assessment.** Images and photographs are evaluated for quality, reliability, and/or clarity. Images were consistently focused and evenly illuminated with a centered optic disc. For the GDx ECC, baseline images had anterior segment retardations of 15 $\mu$m or less. For the HRT II, operators used stereophotographs to assist in drawing the contour line, as they have been shown to improve inter-observer agreement.[30] The mean topography image had a standard deviation of less than 50 $\mu$m. For the Stratus OCT, adequate signal strength (7 or higher) and minimal evidence of algorithm failures was required.

## General fMRI Methodology

BOLD fMRI was used to infer neuronal activity. FMR images were acquired at the Center for Functional Magnetic Resonance Imaging at UCSD with a scanner (3.0-Tesla HD ExciteSigna; General Electric, Milwaukee, WI) with an eight-channel brain coil. Visual stimuli were presented using fiber optic goggles (Avotec Inc., Stuart, FL). The general specifications of the visual presentation system follow: field of view = 30° H (horizontal) × 23° V (vertical); focus ±6 D; maximum luminance, 28.9 cd/m$^2$; resolution, 1024 H × 768 V, and refresh rate, 60 Hz. Visual stimuli were generated by computer (Psychophysics Toolbox[31,32] of MatLab, Mathworks, Natick, MA; PowerBook G4 computer; Apple, Cupertino, CA).

Each subject participated in three 1-hour scanning sessions. An anatomic scan was obtained (FSPGR, 1 × 1 × 1-mm resolution), which served as a reference volume for each subject. For each session, eight functional scans were acquired using a low-bandwidth EPI pulse sequence lasting 260 seconds (130 temporal frames, TR = 2 seconds, TE = 30 ms, flip angle = 90°, 24 coronal slices of 3-mm thickness and 3 × 3-mm resolution, field of view [FOV] = 20 cm). The first 10 temporal frames (20 seconds) were discarded to avoid magnetic saturation effects. Each session ended with another anatomic scan that was used to align functional data across multiple scanning sessions to a subject's reference volume. The occipital pole was flattened initially, and V1 was reflattened after the visual areas (V1, V2, V3) were defined using traditional retinotopy. Cortical flattening techniques and methods for projecting functional data onto the flattened representation have been described in detail elsewhere.[33]

## fMRI Stimuli

The first scanning session for each subject mapped the visual world in retinotopic coordinates on a flattened representation of the cortex using standard stimuli. During a given scan, subjects viewed an expanding ring, a rotating wedge, or a meridian-mapping stimulus composed of alternating hourglass and bowtie patterns. Stimuli were composed from contrast-reversing checkerboards (100% contrast at 8 Hz). The angular velocity of the rotating wedge was 9 deg/s. The speed of the expanding ring was 0.2 deg/s. The spatial frequency of the meridian-mapping stimuli was 0.5 cyc/deg (each square subtending 1° × 1° of visual angle). Stimuli were presented at the center of the screen on a mean gray background, and subjects fixated a target (0.25° × 0.25°) at the center of the screen. The width of the rings was roughly one sixth of their eccentricity, and the polar angle of the wedges was 45°. Stimuli were presented for six 40-second cycles (after discounting the first half cycle, to avoid magnetic saturation effects). Each of three retinotopy stimuli was repeated twice for a total of six functional scans during the first session. The stimulus period (20 seconds on/off) and the temporal frequency of the contrast-reversing checkerboard (8 Hz) were selected from values known to elicit a maximum BOLD response from V1.[34–38]

The second scanning session measured the cortical representation of a 16° isopter in the affected left or right glaucomatous hemifield. Stimuli were made from arcs that extended through the superior (Fig. 1A) or inferior quadrants. Arcs were composed of contrast-reversing checkerboard patterns with a radius of 16° and a width of 2.7°. Each square of the 16° isopter stimuli spanned 7.5° of polar angle. Subjects fixated a target (0.25° × 0.25°) at one corner of the screen while an arc was presented. Each flickering arc was presented alternately with a gray screen every 20 seconds. Four scans measured responses in the superior or inferior quadrants, yielding a total of eight scans. Responses were projected onto the flattened representation of V1 and averaged.

The third scanning session compared viewing through the glaucomatous and fellow eyes. Subjects fixated a target in one corner of the screen while a full-field contrast-reversing checkerboard pattern (Fig. 1B) was presented to the quadrant of visual space with the greatest visual loss. Each square of the scotoma-mapping stimulus subtended 1° × 1° of visual angle. Subjects viewed the "scotoma-mapping" stimulus through each eye in alternating epochs of 20 seconds. The shape of the fixation target indicated which eye should be open.

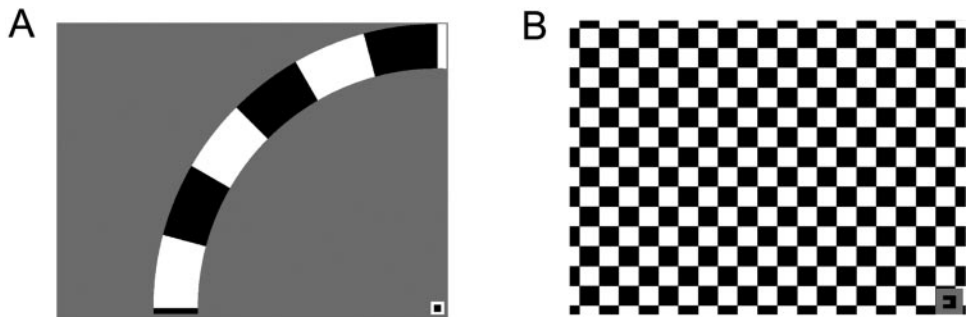


**FIGURE 1.** Visual stimuli for fMRI experiments. Visual stimuli were used to obtain retinotopic maps of the visual world on the flattened cortex. Subjects fixated on a stationary target while contrast-reversing checkerboard patterns (100% contrast, 8 Hz) were presented in the periphery. Standard retinotopic stimuli were used, including expanding rings, rotating wedges, and meridian-mapping stimuli (not pictured). (**A**) Sixteen-degree isopter stimuli. In addition to the standard retinotopy stimuli, the 16° isopter in the hemifield with the greatest visual loss was mapped. A 16° arc subtended the superior or inferior quadrant of the hemifield containing the scotoma. Each arc was presented alternately with a period of no stimulation every half cycle. (**B**) Scotoma-mapping stimulus. A full-field contrast-reversing checkerboard pattern was presented to the quadrant of visual space with the scotoma. Subjects viewed the stimulus through the right or left eye in alternating half cycles.

Eye movements were monitored via an infrared camera in the visual presentation system (iView dark-pupil eye tracking software; SMI, Teltow, Germany). Eye traces were processed according to previously developed protocols.[39] Deviations in eye position beyond 3° of visual angle were flagged. Analysis revealed that the direction of fixation breaks was spatially distributed and not associated with viewing through the glaucomatous or fellow eye ($\chi^2$, all $P > 0.10$). It is important to note that fixation losses only add noise to the fMRI signal. Thus, it is unlikely that fixation losses could account for a correlation between optic disc damage and cortical activity.

## Projecting Patterns of Visual Field Loss onto the Cortex

Responses to the retinotopy stimuli were fitted with templates, which were then used to project regions of visual space onto the flattened representation of cortex.[33] For each subject, the quadrant with the most damage was determined based on the number of SAP test locations that deviated statistically from the normative database (PD greater than 95% confidence limits). The quadrant encompassing that scotoma (Fig. 2 left, bold line) was then projected onto V1 (see Fig. 6E, black line). The projected region of interest (ROI) on the cortex was used to restrict further analysis of the BOLD signal.

Templates were derived from a conformal mapping method developed by Schwartz.[40] Templates were composed of four components representing the 16° isopter, the horizontal meridian, the superior vertical meridian, and the inferior vertical meridian (Fig. 6). Six parameters describe the template; the overall size (*k*), the position (*dx, dy*), the rotation (*da*), the foveal representation (*a*), and the width (*b*).

Templates were fit to the fMRI activity map by adjusting the parameters to maximize the image intensity (i.e., the line integral) under the projected curves. Parameter values from the best-fitting template were obtained by using a nonlinear optimization technique. Templates were then fit to the data using a two-stage optimization routine. In the first stage, each individual model parameter was optimized to fit the template to all activity maps simultaneously. In the second stage, the best-fitting template was generated by simultaneously fitting all parameters to the activity maps. The *k* parameter was excluded from the final optimization because the fit would converge to a single point over a location of maximum amplitude.

The optimized fits for one subject (patient 2) are superimposed on the grayscale activity maps in Figures 6A–D. Colored lines show the fits to response elicited by the 16° isopter and meridian-mapping stimuli. Figure 6E shows the best-fitting template for all stimuli superimposed on the responses to the scotoma-mapping stimulus. Once the best-fitting template was generated for a given subject, the visual quadrant with the scotoma could be projected onto the flattened cortex (black line, Fig. 6E). Further analysis of the BOLD signal was restricted to voxels within the projected ROI.

## Comparing Optic Nerve and fMRI Data

BOLD responses to the scotoma-mapping stimulus were compared to the difference scores from the optic nerve assessment ($GDx_{DIF}$, $HRT_{DIF}$, and $OCT_{DIF}$). Visual fields were used to define the borders of the scotoma that was projected onto the flattened cortical surface (see the Discussion section). Difference scores were computed for each subject as follows. First, the visual *quadrant* with the most extensive loss of visual function was determined with SAP based on the number of PD plot points with triggered probability values. Then, the mean RNFL thickness of the glaucomatous eye was subtracted from that of the fellow eye for the corresponding retinal region (i.e., the retinal region corresponding to the superior or inferior *hemifield*). For example, a difference score for the inferior retinal region would be computed for a subject with superior nasal visual field loss. However, because mean height contour increases with decreasing thickness of the RNFL, the fellow eye was subtracted from the glaucomatous eye to yield an analogous difference score for mean height contour.

The resultant difference scores were then compared to fMRI responses from corresponding regions of visual cortex. Increasingly different values imply a greater deviation from normal vision due to glaucoma. The difference scores were compared with the mean projected amplitudes from the scotoma-mapping experiments, which indicate the difference between viewing through the glaucomatous and fellow eyes.

# Results

## fMRI Data from a Single Subject

The results of SAP are presented for patient 2 (Fig. 2). The SAP results specify that this subject had severe visual loss in the right eye, particularly in the superior visual field. The bold line superimposed on the data for the right eye describes the scotoma selected by the experimenter. The complementary visual quadrant for the left eye is relatively normal.

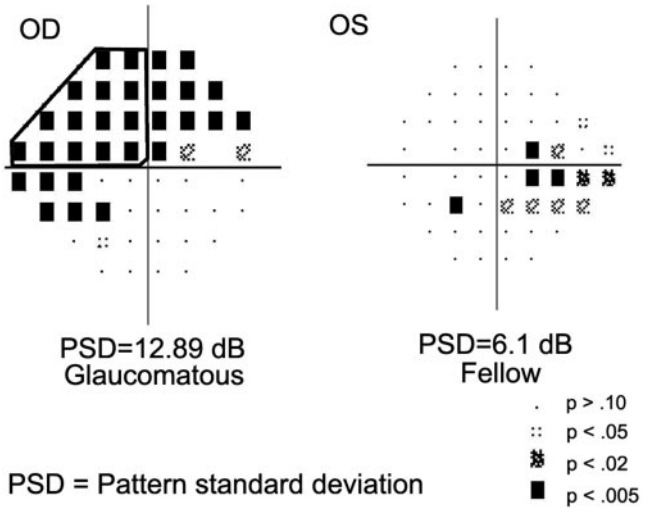


**Figure 2.** Visual field maps. Visual field defects were measured using standard automated perimetry (SAP) and the results for patient 2 are presented. The deviation from the age-corrected normal values is measured in decibels and adjusted for any shifts in overall sensitivity. *PD symbols*: statistical significance of the deviation at each point; *darker symbols*: more significant deviations from the normal thresholds. The pattern SD (PSD) global index describes the SD around the mean of the total deviations. The value is noted below each graph. The experimenter identified the visual quadrant with the greatest vision loss (*bold outline*).

**Scanning Laser Polarimetry.** Excerpts from the GDx ECC printout are displayed in Figure 3 for all six subjects. The retardation image and statistical deviation map from the GDx ECC printout explains the pattern of visual field loss for the example subject (Fig. 3, patient 2). In the retardation maps (top panels), colored pixels indicate the thickness of the RNFL. Yellow and red represent thicker areas, and cool colors (blue and cyan) represent thinner areas. Straight lines define the boundaries of four areas (superior, inferior, nasal, and temporal) in the standard GDx ECC printout. The outer two rings define the borders of the measurement circle. The RNFL for the inferior region of this subject's right eye is thinner relative to the left eye. In the deviation map (bottom panels), colored pixels superimposed on a grayscale retardation image indicate the statistical deviation in RNFL thickness from the normative database. Each superpixel represents the average of 16 individual pixels from the raw data. Only superpixels that are statistically different from the age-matched database receive color. The pattern of superpixels reveals a pronounced decrease in the thickness of the RNFL for the inferior-nasal retinal region of the right eye compared with that of the left eye. This loss of

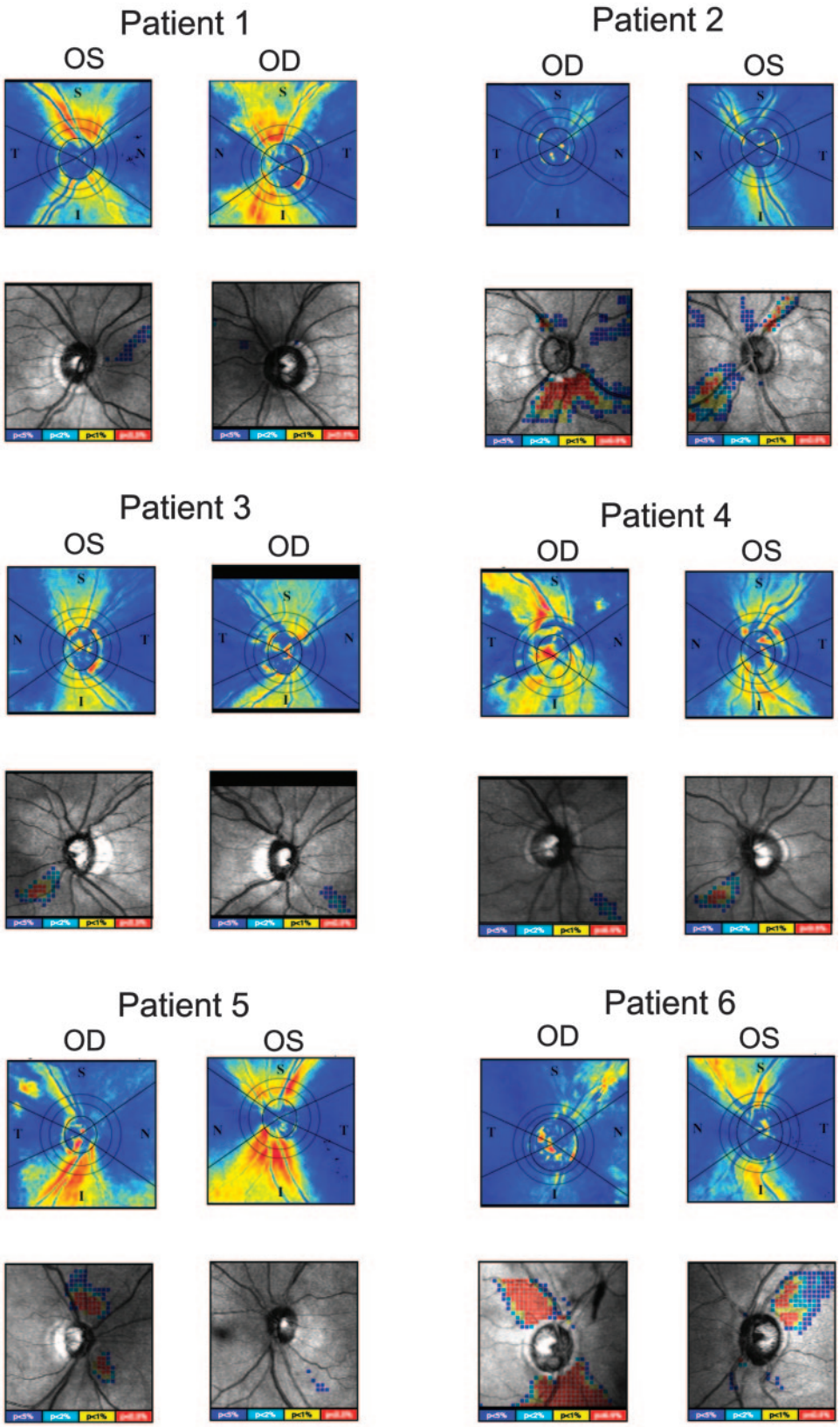


**FIGURE 3.** Scanning laser polarimetry. RNFL thickness was measured by scanning laser polarimetry with ECC (GDx ECC; Carl Zeiss Meditec, Inc.). *Top panels*: retardation images for both eyes. Warm colors indicate regions where RNFL density was thick and cool colors where is was thin. The inferior (I), superior (S), nasal (N), and temporal (T) quadrants of the GDx ECC standard printout are labeled. *Bottom panels*: deviation maps superimposed on grayscale retardation images. *Colored pixels*: statistical deviation in RNFL thickness from the normative database.

retinal nerve fibers is consistent with the visual field loss observed on SAP (Fig. 2).

**Confocal Scanning Laser Ophthalmoscopy.** Excerpts from the HRT II printout are displayed in Figure 4 for all six subjects. The HRT II revealed a similar difference in RNFL thickness and mean height contour between the two eyes of the example subject (Fig. 4, patient 2). The results of the Moorfield's Regression Analysis, which compares the subject's rim area (adjusted relative to disc area) to a normative database internal to the HRT, are presented here for illustrative purposes

only (top panels). The reflectance image of the fundus is artificially colored to portray the topography of the retinal surface. The contour line (green circle) is superimposed on the fundus image along with the boundaries for six polar sectors (white lines). Green checks indicate that the rim area for a given sector is within normal limits (<95th percentile). Yellow exclamation points indicate that the rim area is borderline (95th–99th percentile). Red Xs indicate that the rim area is outside normal limits (>99.9th percentile). There is some evidence of RNFL deterioration in the inferior sectors of the right eye compared with left eye for each of the eight sectors in the contour plot (bottom panels). In these two plots, pie-shaped icons denote area and position of eight sectors. The black lines indicate the height of the contour line around the circumference of the neuroretinal rim (mean height contour). The dark green line indicates the retinal height along the contour line for the normative database. Three zones are colored using the scheme outlined to indicate the relationship between this subject's retinal height and that of the normative database. For the example subject, there is a notable decrease in RNFL thickness (i.e., increased mean height contour) for the inferior sectors of the right eye relative to that for the left eye.

**Optical Coherence Tomography.** Excerpts from the StratusOCT's RNFL Thickness Average Analysis are presented in Figure 5 for all subjects. The digitized image of the parapapillary retina is color-coded to indicate the log reflection intensity of the retinal layers (top panels). Yellow and red denote layers with high reflectance, and cool colors (blue and cyan) denote layers with relatively lower reflectance. The white lines were hand drawn to illustrate the RNFL (Fig. 5, patient 2). The regions surrounding the optic disc are denoted (T, temporal; S, superior; N, nasal; I, inferior). The line graph (bottom) depicts the RNFL thickness for each eye in micrometers as a function of polar angle. Right and left eyes are represented by the solid and dashed lines, respectively. For patient 2, the greatest difference in RNFL thickness between the two eyes is for the

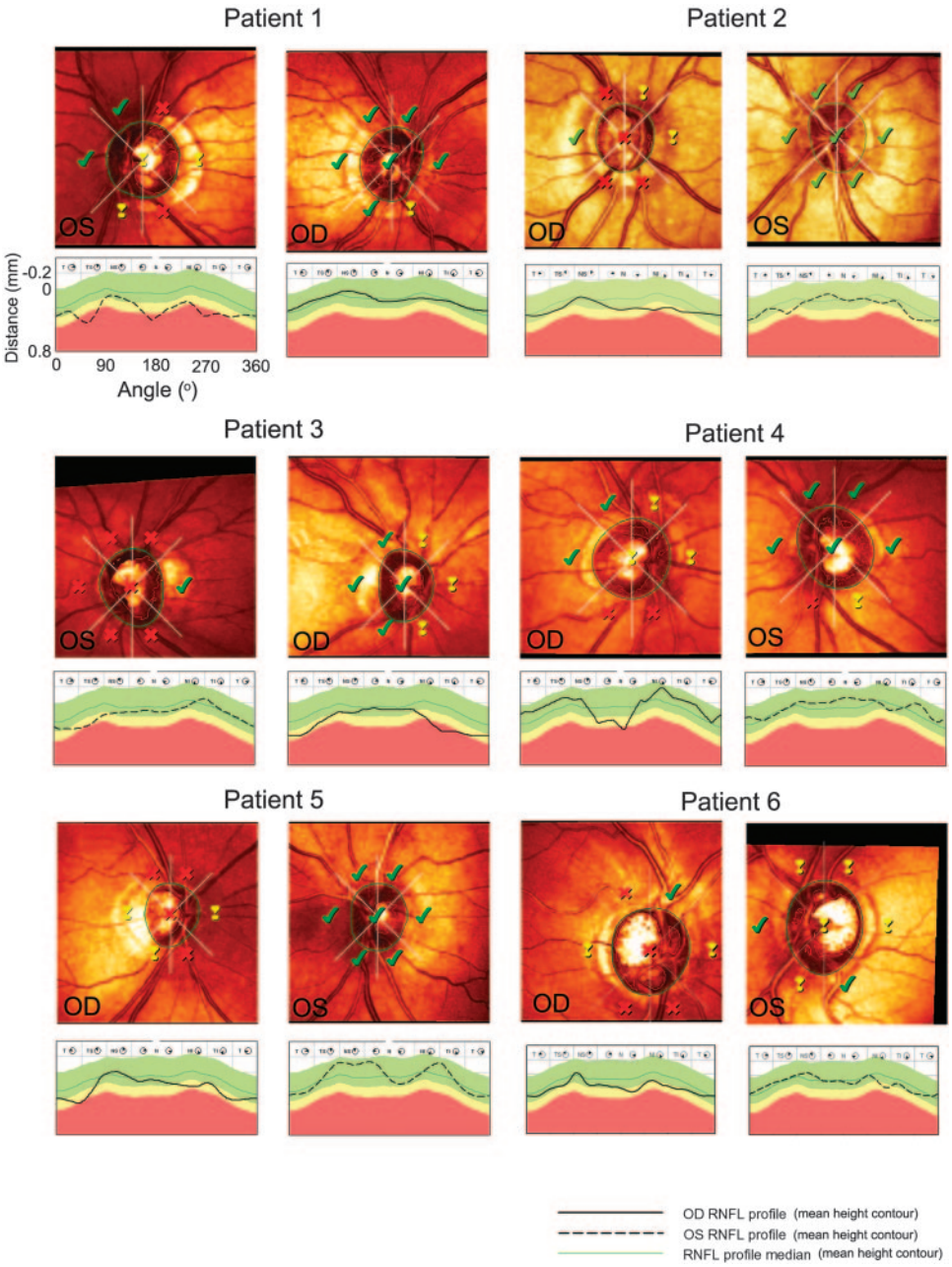


**FIGURE 4.** Confocal scanning laser ophthalmoscopy. Mean height contour and RNFL thickness were measured using the HRT II (Heidelberg Engineering). *Top* panels for each patient show the mean reflectance images that portray the topography of the retinal surface. The contour line (*green*) and the six polar sectors from the Moorfields Regression Analysis (*white lines*) are superimposed on the reflectance images. *Green checks*, *yellow exclamation points*, and *red Xs*: the rim-to-disc area ratio relative to the normative database. *Bottom panels* for each patient show RNFL measurements relative to the normative database. *Pie-shaped icons*: area and position of 45° sectors from the HRT printout. *Black lines*: RNFL thickness; *green line*: median contour line for the normative database. The colored zones (*red*, *yellow*, *green*) relate the RNFL thickness values to the normative database.

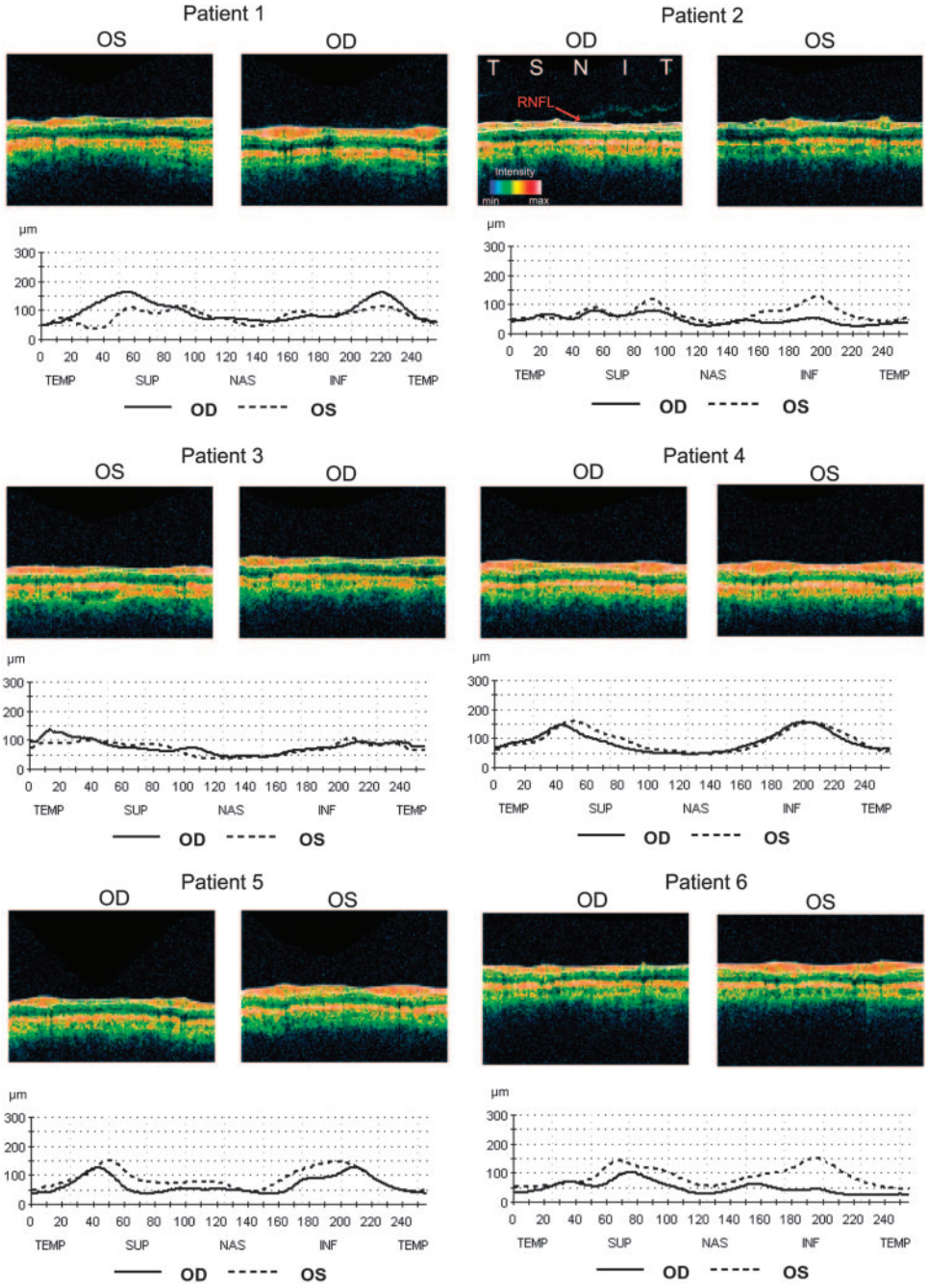


**FIGURE 5.** Optical coherence tomography. Mean RNFL thickness was measured using the StratusOCT (Carl Zeiss Meditec, Inc.). *Top panels* for each patient show a single raw scan of the parapapillary retina for each eye. The log reflection intensity is indicated by the color scheme (patient 2). *Bluish pixels* have less intensity than do *reddish pixels*. *Bottom panels* for each patient show RNFL thickness as a function of polar angle. *Solid lines*: right eyes; *dashed lines*: left eyes.

inferior region, where a loss of fibers in the right eye could be expected based on the results of SAP.

**Functional Magnetic Resonance Imaging.** fMRI responses to retinotopic mapping stimuli for the example subject appear in Figure 6. The inset (bottom right) schematically illustrates the location of the stimuli in visual space. The gray-scale images in each panel show BOLD activity maps on the flattened representation of the right hemisphere. The pattern of BOLD activity (i.e., projected amplitudes) depends on which visual stimulus was presented. Bright regions correspond to locations where changes in BOLD signal correlate positively in time with the stimulus phase (e.g., "on" vs. "off"). The ring-shaped activity (Fig. 6A) shows the BOLD response to the 16° isopter stimuli presented in the left visual hemifield. The red line represents the corresponding component of the best-fitting template for that hemisphere. Similarly, responses to the meridian-mapping stimuli are depicted in Figures 6B–D. The superior (Fig. 6B) and inferior (Fig. 6C) vertical meridians were fit independently, and the best-fitting components from the template are superimposed on the data (light and dark green, respectively). To fit responses to stimulation of the horizontal meridian, the sign of the BOLD response to the meridian-mapping stimulus was simply reversed (Fig. 6D).

The final best-fitting template for this subject is superimposed on the BOLD responses to the scotoma-mapping stimulus (Fig. 6E). The phase of the BOLD response in relation to the temporal phase of monocular viewing is indicated by the color of the pixels. Yellowish pixels correspond to voxels where viewing through the glaucomatous eye resulted in a larger amplitude signal than viewing through the fellow eye. That is to say, fMRI responses were in phase with the glaucomatous eye. Bluish pixels correspond to voxels that were in phase with

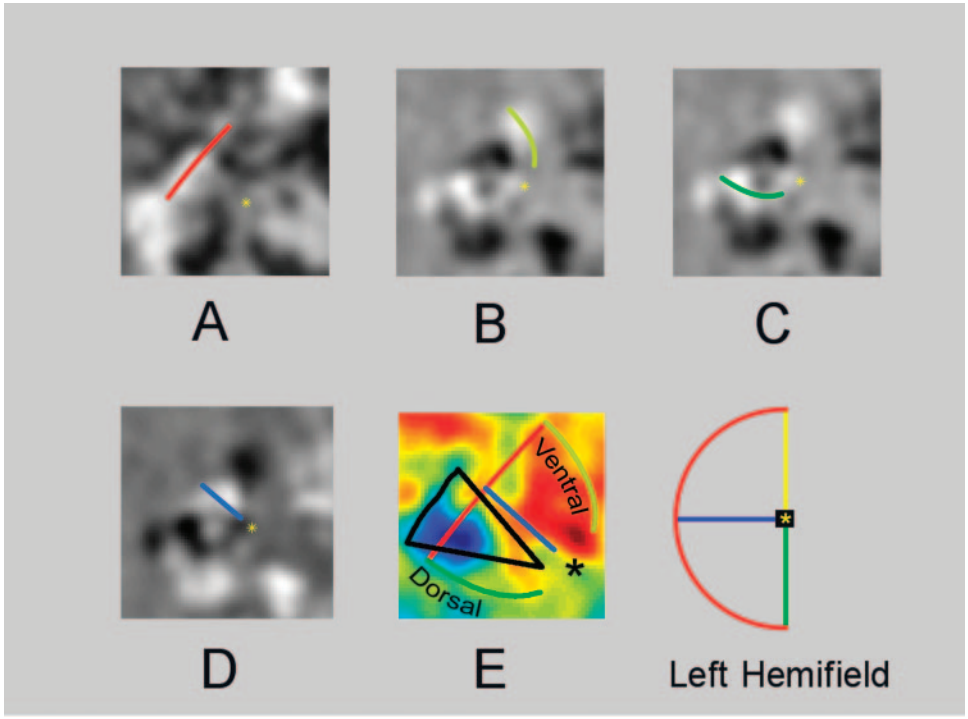


**FIGURE 6.** Cortical responses to retinotopic mapping stimuli for one subject. Grayscale images show BOLD activity maps on the flattened representation of cortex for patient 2. Templates were fit to maximize the image intensity under the projected curves. *Colored lines* are components of the best-fitting template. Components are color coded to match the schematic of visual space in the *inset*. (**A**) Response to the 16° isopter stimuli presented in the left visual hemifield. (**B**) Responses to stimulation of the superior vertical meridian. (**C**) Responses to stimulation of the inferior vertical meridian. (**D**) Responses to stimulation of the horizontal meridian. (**E**) Responses to the scotoma-mapping stimulus. Pixel color indicates the phase of the BOLD response relative to the phase of monocular viewing. *Bluish pixels*: voxels that were in phase with viewing through the fellow eye. *Yellowish pixels*: voxels that were in phase with viewing through the glaucomatous eye. The best-fitting template (*colored lines*) is superimposed on the data. The quadrant with the scotoma is also projected on the flattened representation as an ROI (*black line*). Voxels within the ROI are *blue*, indicating greater BOLD responses when viewing through the fellow eye.

the fellow eye. The template is accompanied by the ROI representing the quadrant of visual space with the most visual loss (black line). Note that the ROI does not completely coincide with the boundaries of V1 that are defined by the template. This discrepancy occurs for two reasons. First, the ROI was selected to circumscribe the test locations of SAP, leaving a small gap between the ROI and the primary meridians. Because there were no test locations abutting the meridians, it was not possible to determine what visual sensitivity would be like there. Hence, the ROI was defined conservatively. Second, conformal mapping is prone to distortions that are more pronounced near the meridians, especially near the fovea. Despite this minor discrepancy, it is quite clear that the ROI is positioned well, and most of the voxels within this ROI are blue, indicating that BOLD responses in the ROI were in phase with viewing through the fellow eye. Furthermore, the mean projected amplitude for voxels within the ROI was significantly different from zero in the direction predicted by the loss of RNFL thickness in the subject's right eye (*t*-test, $P < 0.0001$). Hence, the pattern of deterioration observed with three measures of optic disc structure is reflected by the pattern of BOLD activity in V1.

## FMRI Responses Correlate with Optic Disc Measurements

BOLD responses to the scotoma-mapping stimulus are plotted for all six subjects in Figure 7A. ROIs in the current plot were defined as the region of cortex representing the full quadrant with the scotoma. Mean projected amplitudes for BOLD responses within the ROI were averaged over eight scans per subject. The sign of the BOLD response was normalized (multiplied by 1 or −1) across subjects, depending on which eye was glaucomatous. Error bars show the SEM. Positive numbers indicate that viewing through the fellow eye evoked a larger cortical response than viewing through the glaucomatous eye. Asterisks denote which mean responses were significantly different from zero. Viewing through the fellow eye elicited a significantly greater BOLD response in V1 for four of the six subjects (all $P < 0.01$).

BOLD responses to the scotoma-mapping stimulus were compared to structural measurements of the optic disc in each subject (Figs. 7B–D). In each panel, the mean projected amplitude of the BOLD response is plotted as a function of the interocular difference in (1) RNFL thickness measured with GDx ECC and OCT or (2) mean height contour measured with HRT II. There was a nearly significant correlation between each subject's $GDx_{DIF}$ score and the amplitude of their BOLD response ($r = 0.79$; $P = 0.063$). The correlation between the BOLD responses and the $HRT_{DIF}$ scores for mean height contour was statistically significant ($r = 0.84$, $P = 0.04$), but the correlation with RNFL thickness was not ($r = 0.72$, $P = 0.11$). The correlation for the $OCT_{DIF}$ scores was statistically significant ($r = 0.90$, $P = 0.02$). Moreover, for all three structural tests, there appears to be a consistent trend suggesting that BOLD responses to visual stimulation are related to differences in RNFL thickness or mean height contour between eyes.

It should be noted that there was relatively low power to detect an association for GDx ECC and HRT RNFL thickness (0.60 and 0.49 for GDx ECC and the HRT, respectively) because of the small number of subjects enrolled in the study ($n = 6$). Consequently, a statistical bootstrapping method was used to determine whether the correlations observed between BOLD responses and measurements of the optic disc were real or spurious.[41,42] Statistical bootstrapping is a computer-driven simulation technique for studying the statistics of a population without the need to have the infinite population available. Typically, bootstrapping involves taking random samples (with replacement) from the original dataset and studying how some quantity of interest varies. This technique effectively increases the small sample size of the present study and provides a better estimate of the underlying distribution than traditional approaches. First, the mean projected amplitude of the BOLD

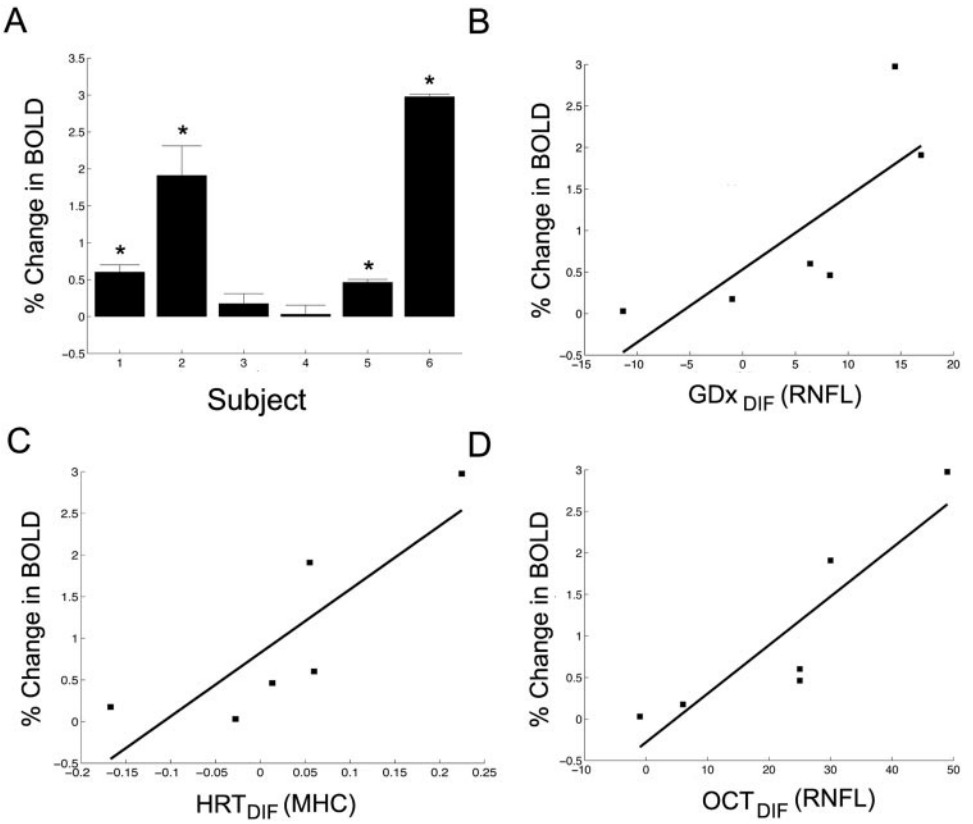


**FIGURE 7.** Cortical responses correlate with optic disc measurements. (**A**) BOLD responses to the scotoma-mapping stimulus in all six subjects. Mean projected amplitudes for BOLD responses within the ROI were averaged over eight scans per subject. Error bars, SEM. Positive numbers indicate that viewing through the fellow eye evoked a larger cortical response than viewing through the glaucomatous eye. *Asterisks:* responses that were statistically different from zero. Four of the six subjects demonstrated significant differences from zero (all $P < 0.01$). (**B**) BOLD responses to the scotoma-mapping stimulus as a function of RNFL thickness measured with the GDx ECC. Difference scores ($GDx_{DIF}$) were computed by subtracting mean RNFL thickness of the glaucomatous eye from that of the fellow eye. The correlation was nearly significant using traditional statistics ($r = 0.79$; $P = 0.06$), due to the small number of subjects (power = 0.60). A statistical bootstrapping analysis indicated that the correlation was significant ($P = 0.008$). (**C**) The correlation between the BOLD responses and the $HRT_{DIF}$ scores for mean height contour was significant, with ($r = 0.84$, $P = 0.01$) and without bootstrapping ($P = 0.04$). (**D**) The correlation for the $OCT_{DIF}$ scores ($r = 0.90$) was also significant, with ($P = 0.002$) and without bootstrapping ($P = 0.02$). Furthermore, the bootstrapping approach shows that observing all three correlation values (GDx, HRT, OCT) by chance was extremely rare ($P = 0.0003$).

response for each subject was randomly paired with the difference scores (i.e., $GDx_{DIF}$, $HRT_{DIF}$, and $OCT_{DIF}$) from another subject. For each sample of random pairings, the correlation coefficients between the BOLD responses and all three difference scores were computed. This process was repeated 10,000 times. To determine the statistical significance (i.e., probability) of each original correlation, the number of randomly generated correlations that exceeded the observed correlation was divided by the total number of random correlations ($n = 10{,}000$). The bootstrapping approach reveals that the BOLD responses correlated significantly with the optic disc measurements of the GDx ($P = 0.008$), the HRT (RNFL, $P = 0.01$; mean height contour, $P = 0.01$), and the OCT ($P = 0.002$). The probability of observing all three original correlations simultaneously was also computed. Accordingly, the number of instances in which the randomly generated sample populations resulted in correlations that concurrently exceeded the observed values for all three structural tests was counted. Then, that number was divided by the total number of randomly generated sample populations ($n = 10{,}000$) to arrive at a probability. The bootstrapping approach shows that observing all three correlation values by chance was extremely rare ($P = 0.0003$). The results are provided in Table 2. The simulations on the data from these six subjects imply that there is a real correlation between the optic disc measurements and BOLD responses to the scotoma-mapping stimulus.

## DISCUSSION

Few studies have been undertaken to investigate the effects of optic neuropathy on the functional organization of LGN or V1 in vivo.[9–17,19–22] One study compared visual field defects to fMRI responses in V1,[22] but the results do not generalize easily to POAG because a heterogeneous population of optic neuropathies was used. The current report is the first to quantify the relationship between measurements of the optic disc and cortical responses in human POAG. Moreover, the results from this study suggest that the ROI template-fitting technique can be used to measure postretinal neurodegeneration in human glaucoma.

### Using Visual Fields to Define Cortical ROIs

There are several reasons why visual fields were chosen over structural scans to define the ROIs in V1. First, the field of view in the MRI scanner was limited to one quadrant. Therefore, it was not possible to compare optic disc measurements for the superior or inferior retinal region to the entire cortical representation of superior or inferior visual space. Second, the relationship between visual fields and optic nerve head topography is not exact. Although certain visual field zones correspond to structural sectors with a high probability, there is considerable variability in this mapping between subjects.[43,44] It would be difficult to determine which portion of the structural scan corresponds to a particular region of cortex. Because of this correspondence problem, the entire superior or inferior retinal region was compared to responses from one cortical quadrant. Third, there is no conformal mapping procedure for the optic nerve head. This problem is closely related to the previous issue. The conformal mapping between visual space and the cortical surface is made possible by a logarithmic transformation. Even if the correspondence between visual fields and optic nerve head structure could be reliably determined, the mapping between the latter and the cortex would

**TABLE 2.** Correlations between BOLD Responses and Measurements of the Optic Disc

| | GDX ECC | HRT (RNFL) | HRT (MHC) | OCT | All Three Combined* |
|---|---|---|---|---|---|
| *P* | 0.008 | 0.01 | 0.01 | 0.002 | 0.0003 |

Results from statistical bootstrapping.
* The probability of observing all three original correlation values simultaneously.

certainly not be logarithmic. Hence, there is no formula to project regions of the optic nerve head onto the cortex. Despite these hindrances, there was evidence of a correlation between optic disc measurements and cortical responses. Continuing developments in conformal mapping and mathematical modeling of optic nerve head topography will allow future comparisons.

## Sources of Potential Error in Template Fitting

Potential sources of error in the template fitting approach have been discussed in detail elsewhere.[33] Computational flattening of the occipital pole, hemodynamic blurring of the BOLD response, and biases introduced by cortical magnification in V1 are potential sources of error. However, these sources do not introduce *systematic* biases into template fitting.[33]

The cortical representation of the fovea is known to be larger than that of the periphery. As a result, fits to the 16° isopter could theoretically be biased toward the fovea. Nonetheless, it was previously demonstrated that increasing the width of annular stimuli with comparable eccentricities does not affect estimates of peak activity in the template fitting protocol.[33]

Minor distortions are inherent in the cortical flattening technique because the surface of the brain is not topologically equivalent to a plane. Distortions were minimized by flattening the smallest region of cortex possible. A ±10% distortion was observed with a roughly equal amount of compression and expansion.[33] Hence, it is unlikely that this method of cortical flattening would introduce a systematic bias in the estimates of V1 topography in subjects with glaucoma. Rather, it would merely increase the variability of the measurement.

## Variability Related to Small Sample Sizes

Despite the small sample size and limited power to detect a correlation between cortical responses and RNFL thickness, consistent trends were reported with relatively strong associations ($r = 0.72–0.90$). Some of these correlations (GDx ECC and HRT RNFL) were just shy of statistical significance, and thus a statistical bootstrapping procedure was also used. This process is accurate[42] and reduces the assumptions made regarding the population distribution.[41] The results of the bootstrapping procedure provide additional evidence for a real correlation between cortical responses and optic disc measurements for all three tests.

The relationship between BOLD response and OCT, GDx ECC, and HRT RNFL measures is consistent with other studies evaluating the discriminating ability of these instruments and their association with visual field damage. For example, although there are often no significant differences among the best OCT, GDx, and RNFL parameters, the OCT has been found to have better (although not necessarily significantly better) discriminating ability between healthy and glaucoma eyes, and a stronger correlation with visual field indices than HRT and GDx.[45] In addition, it has been reported in a few studies that mean height contour has somewhat better discriminating ability[29,46,47] and is more strongly associated with ganglion cell density[48] than with RNFL thickness. The same factors may also explain why OCT had a stronger association with BOLD response than did HRT and GDx measures.

## Visual Field Perimetry Versus Optic Disc Measurements

Preliminary results from our group suggest a correlation between the visual fields of subjects with POAG and cortical responses to the scotoma-mapping stimulus.[23] Three visual function tests were used: SAP, short-wavelength automated perimetry (SWAP), and frequency doubling technology perimetry (FDT). For all three visual function tests, the amplitude of the fMRI response correlated significantly with the difference in PD between eyes. The correlations between cortical activity and SAP ($r = 0.91$) or SWAP ($r = 0.82$) were similar to the correlations between cortical activity and optic disc measurements (0.72–0.90). The correlations were similar despite the fact that visual function tests measure the output of the entire visual system, which is downstream from neural processing in V1. Visual processing in the retina, in contrast, is at least two synapses farther upstream. Optic disc imaging can only estimate the loss of visual function at the retina. Therefore, loss of function further along the visual pathway is not necessarily represented as completely by the RNFL as it would be in perimetry, which requires full system response.

It should also be noted that correlations with the structural measurements in this report may be underestimated because cortical ROIs were not optimally defined (see the section on using visual fields to define cortical ROIs). Visual fields were used to define ROIs in the current experiment, which may also explain why BOLD amplitudes for two subjects were not significant (Fig. 7A). In the previous experiment comparing cortical responses to visual fields, ROIs were defined for each subject according to that individual's scotoma. As a result, the cortical responses for each individual were significant. Despite these differences, the two studies suggest that there may be a relationship between the pattern and severity of visual function loss, the degree and distribution of fiber loss in the RNFL, and the pattern and amplitude of the BOLD response in V1.

## Functional Organization of V1

The current report does not directly address whether V1 undergoes functional reorganization in response to glaucoma. For example, fMRI at 3 T does not have the ability to resolve ocular dominance columns within V1. High-resolution fMRI suggests a majority of the BOLD response originates from ocular dominance columns receiving input from the stimulated eye.[49–52] However, a significant but minor portion of the BOLD response originates from ocular dominance columns receiving input from the nonstimulated eye.[49,51,52] The response from the nonstimulated eye may stem from voxels that reside along the borders of ocular dominance columns or cerebral blood flow that extends across the borders of the ocular dominance columns. Responses may also originate from binocular cells that reside within the columns themselves. The strongest ocular dominance occurs in layer 4c, but other layers have a significant proportion of binocular cells.[53] In addition, long-

range lateral connections are not restricted to columns with the same ocular dominance[54,55] and, feedback projections from layers 6 to 4 do not necessarily project to the same ocular dominance column.[56] Based on results from high-resolution fMRI experiments, the scotoma-mapping experiment should elicit the greatest BOLD response from ocular dominance columns receiving input from the stimulated eye. In the current report, however, the optic disc in both eyes had been affected to some extent by glaucoma. Thus, it is difficult to quantify what proportion of the BOLD response originates from ocular dominance columns receiving input from the stimulated versus nonstimulated eye.

Although fMRI does not have the ability to distinguish between lamina at 3 T, evidence suggests that the BOLD response measured in this report originates predominantly from the input layers of V1. Concurrent extracellular electrophysiological recordings and fMRI measurements of neuronal activity in V1 indicate that the BOLD response originates from the lamina within input layer 4c.[57] In addition, electrophysiological studies in the monkey have shown that the strongest ocular dominance is in layer 4c.[53] Anatomic studies of glaucoma indicate that transynaptic degeneration primarily affects neurons in layer 4c$\beta$.[25] Hence, the BOLD response elicited in the scotoma-mapping experiment most likely originates from—but is not necessarily limited to—layer 4c$\beta$.

It was not possible to measure directly the cortical neurodegeneration in V1, because the BOLD response depended on comparing monocular stimulation of the glaucomatous and fellow eye. This interocular comparison was the best means of comparing the retinotopy on the flattened representation of V1 to interocular differences in damage to the optic disc. Thus, BOLD responses were influenced by damage to the retinal ganglion cell layer in the glaucomatous eye.

Even though glaucomatous neurodegeneration in V1 could not be measured directly with the current paradigm, the results suggest a lack of radical functional reorganization in the cortex. Subjects with glaucoma with severe damage to the optic disc (e.g., patients 2 and 6) demonstrated predictable alterations in retinotopy in corresponding locations of the flattened cortex. These results support recent findings in the monkey, where V1 failed to reorganize after bilateral lesions of the retina.[58] However, the study by Smirnakis et al.[58] only measured functional activity from V1 after 7.5 months, which may still not have been enough time for the cortex to reorganize functionally. Indeed, fMRI studies of macular degeneration demonstrated radical functional reorganization of V1 in response to foveal damage.[59–61] The results in the present study suggest that visual input from the fellow eye (or undamaged regions from both eyes) may be enough to maintain the functional organization of V1.

Future fMRI experiments are planned to assess changes in neuronal activity presumably caused by glaucomatous neurodegeneration in V1. Responses from healthy individuals will be compared to responses from patients with glaucoma who view the scotoma-mapping stimulus through their fellow eye only. Patients with no evidence of glaucomatous degeneration in the fellow eye will be selected. Changes in visually evoked neuronal activity are expected to be less for patients with glaucoma than in control subjects. Furthermore, the relative decrease in activation is expected to be proportional to the amount of damage to the glaucomatous eye.

## Summary

The amplitude of cortical responses in V1 correlated with the difference in structural measurements of the optic disc between glaucomatous and fellow eyes. fMRI may be a useful tool for glaucoma research because it can be used to monitor postretinal neurodegeneration in human glaucoma.

## *Acknowledgments*

The authors thank Wade Wong, DO, for reviewing the anatomic reference volumes for evidence of untoward pathology along the retinocortical pathway.

## *References*

1. Friedman DS, Wolfs RC, O'Colmain BJ, et al. Prevalence of open-angle glaucoma among adults in the United States. *Arch Ophthalmol.* 2004;122:532–538.
2. Weinreb RN, Khaw PT. Primary open-angle glaucoma. *Lancet.* 2004;363:1711–1720.
3. Fechtner RD, Weinreb RN. Mechanisms of optic nerve damage in primary open angle glaucoma. *Surv Ophthalmol.* 1994;39:23–42.
4. Weber AJ, Chen H, Hubbard WC, Kaufman PL. Experimental glaucoma and cell size, density, and number in the primate lateral geniculate nucleus. *Invest Ophthalmol Vis Sci.* 2000;41:1370–1379.
5. Yucel YH, Zhang Q, Gupta N, Kaufman PL, Weinreb RN. Loss of neurons in magnocellular and parvocellular layers of the lateral geniculate nucleus in glaucoma. *Arch Ophthalmol.* 2000;118:378–384.
6. Yucel YH, Zhang Q, Weinreb RN, Kaufman PL, Gupta N. Atrophy of relay neurons in magno- and parvocellular layers in the lateral geniculate nucleus in experimental glaucoma. *Invest Ophthalmol Vis Sci.* 2001;42:3216–3222.
7. Crawford ML, Harwerth RS, Smith EL 3rd, Mills S, Ewing B. Experimental glaucoma in primates: changes in cytochrome oxidase blobs in V1 cortex. *Invest Ophthalmol Vis Sci.* 2001;42:358–364.
8. Yucel YH, Zhang Q, Weinreb RN, Kaufman PL, Gupta N. Effects of retinal ganglion cell loss on magno-, parvo-, koniocellular pathways in the lateral geniculate nucleus and visual cortex in glaucoma. *Prog Retin Eye Res.* 2003;22:465–481.
9. Goldberg I, Graham SL, Klistorner AI. Multifocal objective perimetry in the detection of glaucomatous field loss. *Am J Ophthalmol.* 2002;133:29–39.
10. Graham SL, Klistorner AI, Goldberg I. Clinical application of objective perimetry using multifocal visual evoked potentials in glaucoma practice. *Arch Ophthalmol.* 2005;123:729–739.
11. Graham SL, Klistorner AI, Grigg JR, Billson FA. Objective VEP perimetry in glaucoma: asymmetry analysis to identify early deficits. *J Glaucoma.* 2000;9:10–19.
12. Hasegawa S, Ohshima A, Hayakawa Y, Takagi M, Abe H. Multifocal electroretinograms in patients with branch retinal artery occlusion. *Invest Ophthalmol Vis Sci.* 2001;42:298–304.
13. Hood DC, Greenstein VC. Multifocal VEP and ganglion cell damage: applications and limitations for the study of glaucoma. *Prog Retin Eye Res.* 2003;22:201–251.
14. Hood DC, Thienprasiddhi P, Greenstein VC, et al. Detecting early to mild glaucomatous damage: a comparison of the multifocal VEP and automated perimetry. *Invest Ophthalmol Vis Sci.* 2004;45:492–498.
15. Hood DC, Zhang X, Greenstein VC, et al. An interocular comparison of the multifocal VEP: a possible technique for detecting local damage to the optic nerve. *Invest Ophthalmol Vis Sci.* 2000;41:1580–1587.
16. Klistorner AI, Graham SL, Grigg JR, Billson FA. Multifocal topographic visual evoked potential: improving objective detection of local visual field defects. *Invest Ophthalmol Vis Sci.* 1998;39:937–950.
17. Thienprasiddhi P, Greenstein VC, Chen CS, Liebmann JM, Ritch R, Hood DC. Multifocal visual evoked potential responses in glaucoma patients with unilateral hemifield defects. *Am J Ophthalmol.* 2003;136:34–40.
18. Fortune B, Hood DC. Conventional pattern-reversal VEPs are not equivalent to summed multifocal VEPs. *Invest Ophthalmol Vis Sci.* 2003;44:1364–1375.
19. Kiyosawa M, Bosley TM, Kushner M, et al. Positron emission tomography to study the effect of eye closure and optic nerve damage on human cerebral glucose metabolism. *Am J Ophthalmol.* 1989;108:147–152.

20. Sugiyama T, Utsunomiya K, Ota H, Ogura Y, Narabayashi I, Ikeda T. Comparative study of cerebral blood flow in patients with normal-tension glaucoma and control subjects. *Am J Ophthalmol*. 2006;141:394–396.
21. Yoshida Y, Sugiyama T, Sugasawa J, Nakajima M, Ikeda T, Utsunomiya K. A case of normal-tension glaucoma with impaired eye movements in a young patient (in Japanese). *Nippon Ganka Gakkai Zasshi*. 2006;110:477–483.
22. Miki A, Nakajima T, Takagi M, Shirakashi M, Abe H. Detection of visual dysfunction in optic atrophy by functional magnetic resonance imaging during monocular visual stimulation. *Am J Ophthalmol*. 1996;122:404–415.
23. Duncan RO, Sample PA, Weinreb RN, Bowd C, Zangwill LM. Retinotopic organization of primary visual cortex in glaucoma: comparing fMRI measurements of cortical function with visual field loss. *Prog Retin Eye Res.* 2007;26:38–56.
24. Harwerth RS, Carter-Dawson L, Shen F, Smith EL 3rd, Crawford ML. Ganglion cell losses underlying visual field defects from experimental glaucoma. *Invest Ophthalmol Vis Sci*. 1999;40:2242–2250.
25. Crawford ML, Harwerth RS, Smith EL 3rd, Shen F, Carter-Dawson L. Glaucoma in primates: cytochrome oxidase reactivity in parvo- and magnocellular pathways. *Invest Ophthalmol Vis Sci*. 2000;41:1791–1802.
26. Medeiros FA, Zangwill LM, Bowd C, Vessani RM, Susanna R Jr, Weinreb RN. Evaluation of retinal nerve fiber layer, optic nerve head, and macular thickness measurements for glaucoma detection using optical coherence tomography. *Am J Ophthalmol*. 2005;139:44–55.
27. Medeiros FA, Zangwill LM, Bowd C, Weinreb RN. Comparison of the GDx VCC scanning laser polarimeter, HRT II confocal scanning laser ophthalmoscope, and Stratus OCT optical coherence tomograph for the detection of glaucoma. *Arch Ophthalmol*. 2004;122:827–837.
28. Zhou Q, Knighton R. Nerve Fibre Analyzer GDx: New Techniques. In: Iester M, Garway-Heath D, Lemij H, eds. *Optic Nerve Head and Retinal Nerve Fibre Analysis.* Savona, Italy: Dogma; 2005;117–119.
29. Zangwill LM, Weinreb RN, Beiser JA, et al. Baseline topographic optic disc measurements are associated with the development of primary open-angle glaucoma: the Confocal Scanning Laser Ophthalmoscopy Ancillary Study to the Ocular Hypertension Treatment Study. *Arch Ophthalmol*. 2005;123:1188–1197.
30. Iester M, Mikelberg FS, Courtright P, et al. Interobserver variability of optic disk variables measured by confocal scanning laser tomography. *Am J Ophthalmol*. 2001;132:57–62.
31. Brainard DH. The Psychophysics Toolbox. *Spat Vis*. 1997;10:433–436.
32. Pelli DG. The VideoToolbox software for visual psychophysics: transforming numbers into movies. *Spat Vis*. 1997;10:437–442.
33. Duncan RO, Boynton GM. Cortical magnification within human primary visual cortex correlates with acuity thresholds. *Neuron*. 2003;38:659–671.
34. DeYoe EA, Bandettini P, Neitz J, Miller D, Winans P. Functional magnetic resonance imaging (FMRI) of the human brain. *J Neurosci Methods*. 1994;54:171–187.
35. Engel SA, Glover GH, Wandell BA. Retinotopic organization in human visual cortex and the spatial precision of functional MRI. *Cereb Cortex*. 1997;7:181–192.
36. Engel SA, Rumelhart DE, Wandell BA, et al. fMRI of human visual cortex. *Nature*. 1994;369:525.
37. Sereno MI, Dale AM, Reppas JB, et al. Borders of multiple visual areas in humans revealed by functional magnetic resonance imaging. *Science*. 1995;268:889–893.
38. Tootell RB, Hadjikhani NK, Vanduffel W, et al. Functional analysis of primary visual cortex (V1) in humans. *Proc Natl Acad Sci USA*. 1998;95:811–817.
39. Krauzlis RJ, Miles FA. Initiation of saccades during fixation or pursuit: evidence in humans for a single mechanism. *J Neurophysiol*. 1996;76:4175–4179.
40. Schwartz EL. A quantitative model of the functional architecture of human striate cortex with application to visual illusion and cortical texture analysis. *Biol Cybern*. 1980;37:63–76.
41. Henderson AR. The bootstrap: a technique for data-driven statistics: using computer-intensive analyses to explore experimental data. *Clin Chim Acta*. 2005;359:1–26.
42. Hesterberg T, Moore DS, Monaghan S, Clipson A, Epstein R. *Bootstrap Methods and Permutation Tests.* 2nd ed. New York: WH Freeman; 2005.
43. Garway-Heath DF, Poinoosawmy D, Fitzke FW, Hitchings RA. Mapping the visual field to the optic disc in normal tension glaucoma eyes. *Ophthalmology*. 2000;107:1809–1815.
44. Anton A, Yamagishi N, Zangwill L, Sample PA, Weinreb RN. Mapping structural to functional damage in glaucoma with standard automated perimetry and confocal scanning laser ophthalmoscopy. *Am J Ophthalmol*. 1998;125:436–446.
45. Bowd C, Zangwill LM, Medeiros FA, et al. Structure-function relationships using confocal scanning laser ophthalmoscopy, optical coherence tomography and scanning laser polarimetry. *Invest Ophthalmol Vis Sci.* 2006;47:2889–2995.
46. Mardin CY, Horn FK, Jonas JB, Budde WM. Preperimetric glaucoma diagnosis by confocal scanning laser tomography of the optic disc. *Br J Opbthalmol*. 1999;83:299–304.
47. Zangwill LM, Chan K, Bowd C, et al. Heidelberg retina tomograph measurements of the optic disc and parapapillary retina for detecting glaucoma analyzed by machine learning classifiers. *Invest Ophthalmol Vis Sci*. 2004;45:3144–3151.
48. Yucel YH, Gupta N, Kalichman MW, et al. Relationship of optic disc topography to optic nerve fiber number in glaucoma. *Arch Ophthalmol*. 1998;116:493–497.
49. Cheng K, Waggoner RA, Tanaka K. Human ocular dominance columns as revealed by high-field functional magnetic resonance imaging. *Neuron*. 2001;32:359–374.
50. Dechent P, Frahm J. Direct mapping of ocular dominance columns in human primary visual cortex. *Neuroreport*. 2000;11:3247–3249.
51. Menon RS, Goodyear BG. Submillimeter functional localization in human striate cortex using BOLD contrast at 4 Tesla: implications for the vascular point-spread function. *Magn Reson Med*. 1999;41:230–235.
52. Menon RS, Ogawa S, Strupp JP, Ugurbil K. Ocular dominance in human V1 demonstrated by functional magnetic resonance imaging. *J Neurophysiol*. 1997;77:2780–2787.
53. Hubel DH, Wiesel TN. Receptive fields and functional architecture of monkey striate cortex. *J Physiol*. 1968;195:215–243.
54. Malach R, Amir Y, Harel M, Grinvald A. Relationship between intrinsic connections and functional architecture revealed by optical imaging and in vivo targeted biocytin injections in primate striate cortex. *Proc Natl Acad Sci USA*. 1993;90:10469–10473.
55. Yoshioka T, Blasdel GG, Levitt JB, Lund JS. Relation between patterns of intrinsic lateral connectivity, ocular dominance, and cytochrome oxidase-reactive regions in macaque monkey striate cortex. *Cereb Cortex*. 1996;6:297–310.
56. Wiser AK, Callaway EM. Ocular dominance columns and local projections of layer 6 pyramidal neurons in macaque primary visual cortex. *Vis Neurosci*. 1997;14:241–251.
57. Logothetis NK, Pauls J, Augath M, Trinath T, Oeltermann A. Neurophysiological investigation of the basis of the fMRI signal. *Nature*. 2001;412:150–157.
58. Smirnakis SM, Brewer AA, Schmid MC, et al. Lack of long-term cortical reorganization after macaque retinal lesions. *Nature*. 2005;435:300–307.
59. Baker CI, Peli E, Knouf N, Kanwisher NG. Reorganization of visual processing in macular degeneration. *J Neurosci*. 2005;25:614–618.
60. Nguyen TH, Stievenart JL, Saucet JC, et al. Cortical response to age-related macular degeneration. Part II: functional MRI study (in French). *J Fr Ophtalmol.* 2004;27:3S72–S86.
61. Nguyen TH, Stievenart JL, Saucet JC, et al. Cortical response in age-related macular degeneration. Part I: methodology and subject specificities (in French). *J Fr Ophtalmol.* 2004;27:3S65–S71.